ACS Energy LETTERS

http://pubs.acs.org/journal/aelccp

All-Perovskite Tandems Enabled by Surface Anchoring of Long-Chain Amphiphilic Ligands

Aidan Maxwell,[†] Hao Chen,[†] Luke Grater, Chongwen Li, Sam Teale, Junke Wang, Lewei Zeng, Zaiwei Wang, So Min Park, Maral Vafaie, Siraj Sidhik, Isaac W. Metcalf, Yanjiang Liu, Aditya D. Mohite, Bin Chen,* and Edward H. Sargent*

Cite This: *ACS Energy Lett.* 2024, 9, 520−527

Read Online

ACCESS | Metrics & More | Article Recommendations | Supporting Information

ABSTRACT: **Perovskite solar cells (PSCs) in the *pin* structure are limited by nonradiative recombination at the electron transport layer (ETL) interface, which is exacerbated in narrow-bandgap (∼1.2 eV) Pb−Sn PSCs due to surface Sn oxidation and detrimental p-doping. Photoluminescence quantum yield studies herein indicated that ethane-1,2-diammonium (EDA) passivation only partially alleviates perovskite/ETL energetic losses. We pursued passivation of the defect-rich perovskite:ETL interface to reduce nonradiative losses; our target was to combine chemical coordination of Sn sites with the introduction of an interlayer, which we implemented by introducing long-chain carboxylic acid ligands at the perovskite surface. Treatment with oleic acid (OA) led to reduced recombination at the perovskite/ETL interface and evidence of Sn^{2+} coordination. This reduced the V_{OC} deficit of Pb−Sn PSCs to 0.34 V, resulting in a 0.89 V V_{OC} and PCE of 23.0% (22.4% stabilized). Incorporating the OA-treated Pb−Sn layer into a monolithic all-perovskite tandem, we report a 27.3% PCE (26.4% certified) and a V_{OC} of 2.21 V.**

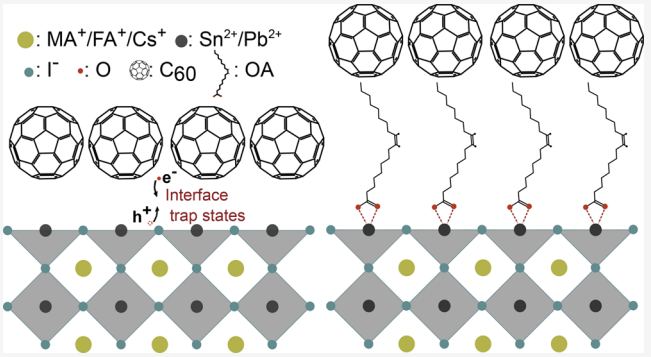

Bandgap tuning in metal-halide perovskites (∼1.2−3.0 eV) has resulted in their integration into tandem solar cells with silicon, copper indium gallium selenide (CIGS), and organic photovoltaics.[1−4] Showing particular promise as the small-gap subcell in tandems are narrow-bandgap (NBG) ∼1.2 eV perovskites fabricated by B-site alloying of Pb and Sn.[5−7] All-perovskite tandems have recently surpassed the record certified power conversion efficiency (PCE) reported in single-junction perovskite solar cells (PSCs).[8−10]

PCE retains nevertheless the potential for further improvement; in particular, the open-circuit voltage (V_{OC}) lies appreciably below its theoretical limit.[11−13] Losses in device V_{OC} have been shown to stem from nonradiative recombination at the interfaces between perovskite and charge transport layers; this is seen as a reduction in perovskite photoluminescence quantum yield (PLQY) after contact with charge transport layers.[14,15] It appears that recombination pathways are introduced at the perovskite/transport-layer interface. C_{60}, an electron transport layer (ETL) widely used in inverted (*pin*) PSCs, is one of the worst offenders when it comes to the introduction of these trap states. It has been reported that even ∼1 nm of C_{60} deposited onto the perovskite surface can result in a reduction in PLQY by several orders of magnitude, pointing to the nm-scale interface point of contact between the perovskite and C_{60}, rather than in the bulk of either layer.[14] Strategies to mitigate this interfacial recombination have included surface defect passivation, post-treatments with divalent cations for the introduction of a surface dipole to reduce minority carrier concentration (analogous to field-effect passivation), and the introduction of an insulating interlayer to physically separate the perovskite and C_{60}.[10,15−18]

The phenomenon appears even more acute in NBG perovskites: in mixed Pb−Sn PSCs, a larger conduction band offset with C_{60} results in difficulty introducing energetically aligned interlayers between the perovskite and ETL.[17,19] Additionally, Sn^{2+} at the ETL-facing top surface of the perovskite oxidizes readily to Sn^{4+} in the presence of air and moisture; this results in p-doping, increasing thereby the concentration of minority carriers near the ETL interface.[20−22]

Received: November 15, 2023
Revised: January 12, 2024
Accepted: January 17, 2024
Published: January 23, 2024

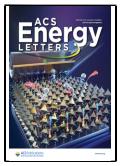

Downloaded via UNIV OF OXFORD on March 29, 2026 at 02:00:44 (UTC).
See https://pubs.acs.org/sharingguidelines for options on how to legitimately share published articles.

ACS Publications

© 2024 American Chemical Society

https://doi.org/10.1021/acsenergylett.3c02470
ACS Energy Lett. 2024, 9, 520−527

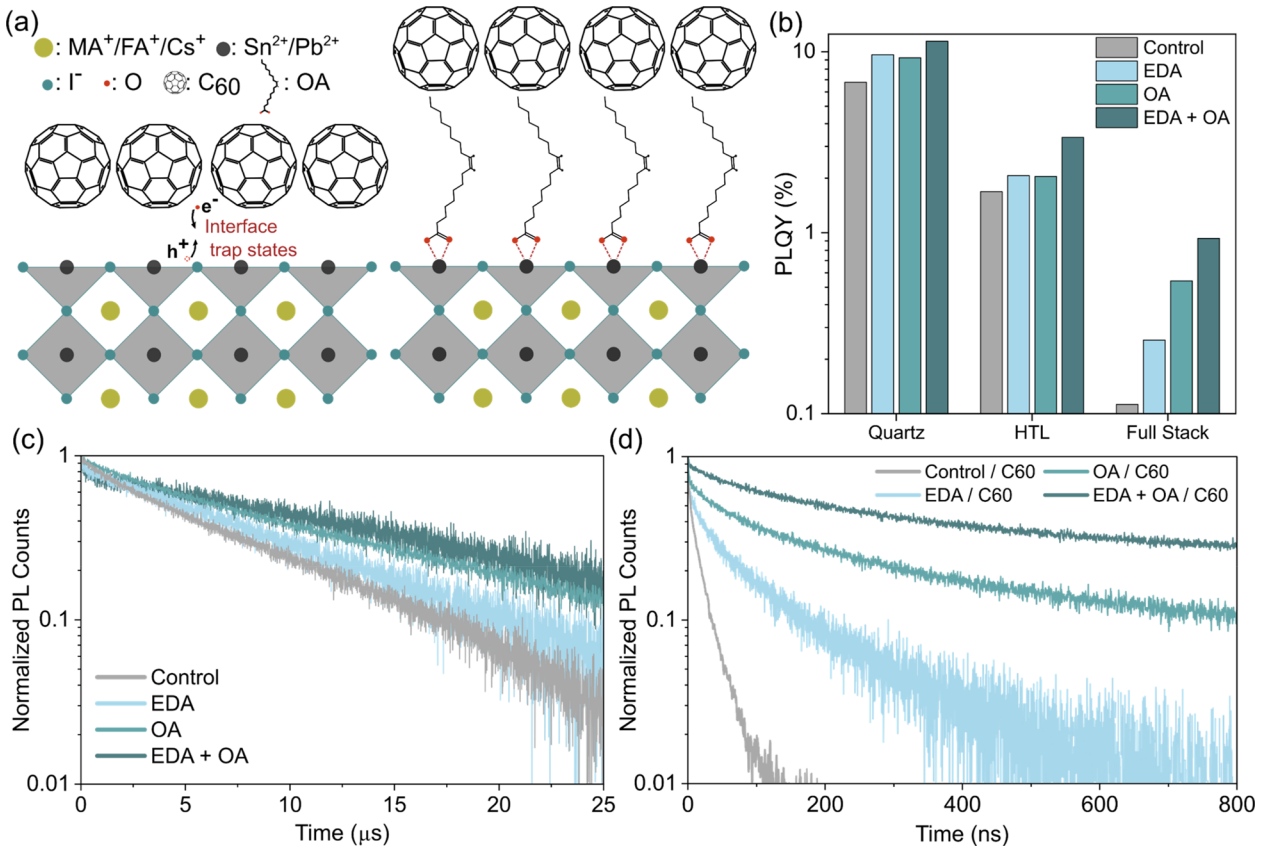

Figure 1. Reduced recombination at the perovskite/ETL interface. (a) Schematic diagram of the perovskite/C_{60} interface (left) and the perovskite/C_{60} interface with an interlayer of OA preventing direct contact and reducing minority carrier interface recombination (right). (b) PLQY data from control (untreated), EDA, OA, and EDA+OA treated films on quartz and PEDOT:PSS (HTL) substrates, as well as full device stacks (PEDOT:PSS/perovskite/C_{60}). (c) Transient photoluminescence traces for control (untreated), EDA, OA, and EDA+OA treated films on quartz substrates. (d) Transient photoluminescence traces for control (untreated), EDA, OA, and EDA+OA treated films on quartz substrates with a layer of C_{60} deposited on top. The lifetimes for each trace were calculated and can be found in Supplementary Table S1. All films were encapsulated to avoid environmentally induced degradation.

To address these challenges simultaneously, researchers making high-performing Pb−Sn PSCs have relied on post-treatment using diammonium ligands such as ethane-1,2-diammonium diiodide (EDA^{2+}, hereafter referred to as EDA for simplicity), the diammonium counterpart to ethylenediamine, which induce n-type doping at the perovskite surface and favorable conduction band-bending.[17,23−26] This strategy does significantly reduce V_{OC} losses in Pb−Sn PSCs (≥34 mV),[25] yet V_{OC} deficits remain larger than those of conventional ∼1.5 eV Pb-based perovskites, which have achieved V_{OC} deficits approaching 0.30 V.[27]

We posited that further efforts to provide a controlled separation between ETL and NBG perovskite, a separation strategy also providing chemical passivation of the perovskite surface, could offer a route to further increases in V_{OC}. We hypothesized that a polar carboxylic acid functional group could coordinate Sn^{2+}/Pb^{2+} on the perovskite surface providing passivation,[28−30] while a nonpolar carbon chain could improve contact with the nonpolar C_{60} and act as an interlayer, avoiding the direct contact that has been shown to introduce trap states and minority carrier interface recombination (Figure 1a).[14,16,18]

We began by screening various ligands to elucidate the effects of various polar functional groups and nonpolar carbon chain lengths on NBG device performance. In particular, we tested 0.5, 1.5, and 5 mM surface treatment solutions of oleic acid (OA), dodecanoic acid (DA), 12-hydroxydodecanoic acid (DAOH), N-dodecylammonium iodide (NDAI), and butyric acid (BA) compared to control, untreated PbSn devices (Figures S1 and S2). We observed a positive correlation between the length and hydrophobicity of the carbon chain and device performance. We also observe that treatment with DA, the carboxylic acid counterpart to NDAI, results in higher V_{OC} and PCE than treatment with NDAI. OA, with both a long nonpolar carbon chain and a carboxylic acid functional group, provided the most significant performance enhancement. Thus, we shifted our focus to OA, a long-chain amphiphilic ligand commonly used as a surface agent to stabilize quantum dots and nanoparticles.[31−34] While treatments with OA have been investigated previously in Pb-based perovskite solar cells to a limited extent,[35,36] it was unclear whether their benefits extended to mixed PbSn perovskites with distinct surface chemistry. To evaluate the effects of OA treatment in comparison with state-of-the-art diammonium passivation strategies, we used EDA-treated Pb−Sn perovskites as our control samples for each of the following characterizations.

First, we spin-coated 1.8 M $Cs_{0.05}FA_{0.7}MA_{0.25}Pb_{0.5}Sn_{0.5}I_3$ films atop quartz and quartz/hole transport layer (HTL) substrates using PEDOT:PSS as the HTL and measured the PLQY of each variation in addition to that of full device stacks with a C_{60} (ETL) layer (HTL/perovskite/ETL). In this study,

https://doi.org/10.1021/acsenergylett.3c02470
ACS Energy Lett. 2024, 9, 520−527

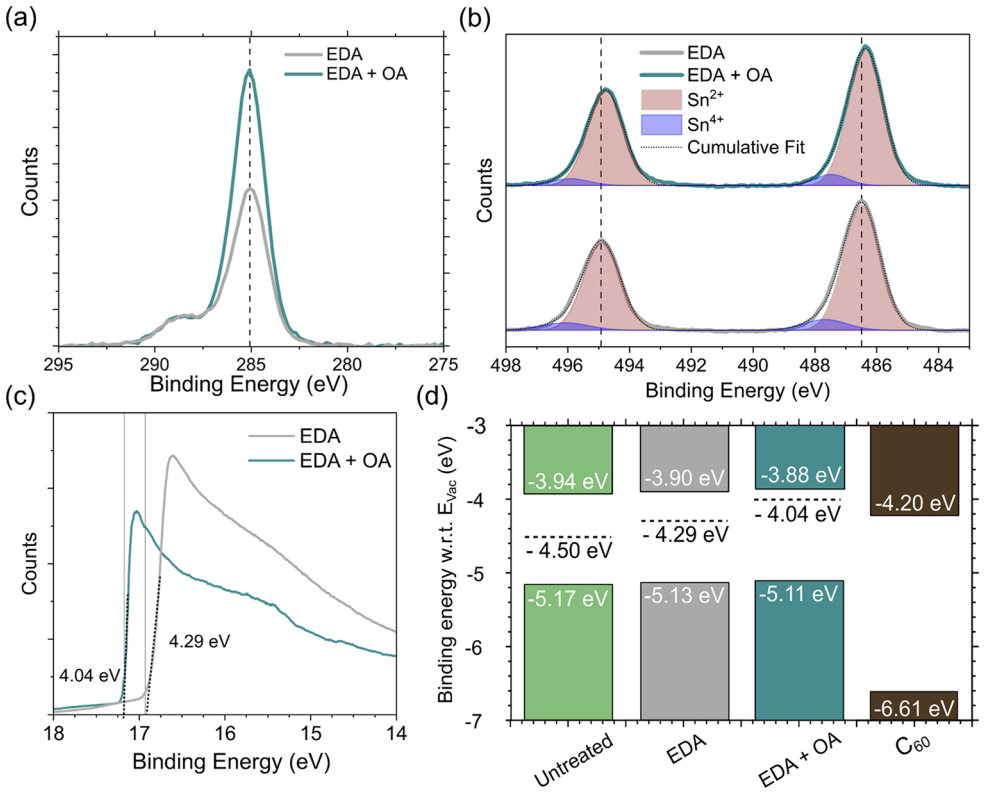

Figure 2. Surface coordination and n-doping effects of OA post-treatment. (a) XPS spectra of C 1s core levels for EDA and EDA+OA-treated films. (b) XPS spectra of Sn 3d core levels for EDA and EDA+OA-treated films. (c) UPS spectra showing the low-KE cutoff of EDA and EDA +OA-treated films. Fermi edge UPS data are shown in Figure S10. (d) Band alignment diagrams of untreated, EDA-treated, and EDA+OA-treated films compared with C_{60}.

our control films were not post-treated, whereas our target films compared post-treatments with solutions of EDA, OA, and a combination of EDA and OA (EDA+OA) (Figure 1b). We found that each of the post-treatment variations resulted in only slight improvements in PLQY of perovskite films on quartz and HTL substrates. However, while the control perovskite film exhibits a drop in PLQY of nearly 2 orders of magnitude upon the addition of C_{60} (full stack), each of the post-treatments significantly reduces the magnitude of these losses. Interestingly, we note that although treatment with OA results in a PLQY similar to that of EDA for neat perovskite films on quartz and PEDOT:PSS substrates, the OA treatment is more effective at suppressing C_{60}-induced interface losses. Furthermore, we observe a synergistic interface passivation effect between EDA and OA; the combination of EDA+OA treatment results in the highest PLQY for full HTL/perovskite/ETL material stacks.

To investigate further the effects of OA treatment on the bulk and interfacial carrier dynamics, we carried out time-resolved photoluminescence (TRPL) measurements of Pb−Sn films and device stacks (Figure 1c,d and Figure S3). In the case of bare perovskite films on quartz, OA treatment did not have a significant additional impact on carrier lifetimes, with EDA and EDA+OA-treated films exhibiting weighted average lifetimes (τ) of 8 and 11 μs, respectively (Supplementary Table S1, Supplementary Note 1). However, upon addition of a C_{60} film on the perovskite layer, OA-treated perovskite/C_{60} stacks exhibited significantly longer carrier lifetimes when illuminated from the top surface (i.e., generating carriers closer to the C_{60} interface), due to a longer τ_2 which is indicative of reduced nonradiative recombination.[37] When we illuminated from the bottom (quartz) surface and thus sought to generate carriers further from the C_{60} interface, both the EDA and EDA+OA-treated perovskite/ETL stacks exhibited longer carrier lifetimes more comparable to that of the bare perovskite films on quartz (Figure S3a).

Seeking to investigate the effects of OA on the crystallographic structure of the Pb−Sn perovskite and determine whether a 2D perovskite phase is formed during surface treatment, we carried out grazing incidence wide-angle X-ray scattering (GIWAXS) and transient reflection (TR) spectroscopy (Figures S4 and S5). While GIWAXS spectra show evidence of PbI_2 formation after EDA treatment, seen in the shoulder of the (100) peak at ∼1.0 Å indicative of surface degradation under ambient conditions,[10] no peaks consistent with a 2D perovskite phase after OA treatment were present at the surface. Similarly, the TR spectra display only the absorption from the 3D perovskite phase (∼1000 nm) with no additional bleach peaks in the 700−900 nm range as would be expected for a 2D surface layer.[38] X-ray diffraction (XRD) patterns of untreated, EDA-treated, and EDA+OA-treated PbSn films on ITO also showed no changes to the bulk perovskite crystal structure (Figure S6). Scanning electron microscopy (SEM) images further corroborated the lack of any significant changes to surface morphology after post-treatment with OA (Figure S7). The control film however contains some deposits which can be attributed to SnF_2,[25] which appear to be washed away after the perovskite films are post-treated with OA solution.

We turned next to X-ray photoelectron spectroscopy (XPS) of EDA and EDA+OA-treated perovskite films exposed to air for 1 min, to look for evidence of OA on the perovskite surface

https://doi.org/10.1021/acsenergylett.3c02470
ACS Energy Lett. 2024, 9, 520−527

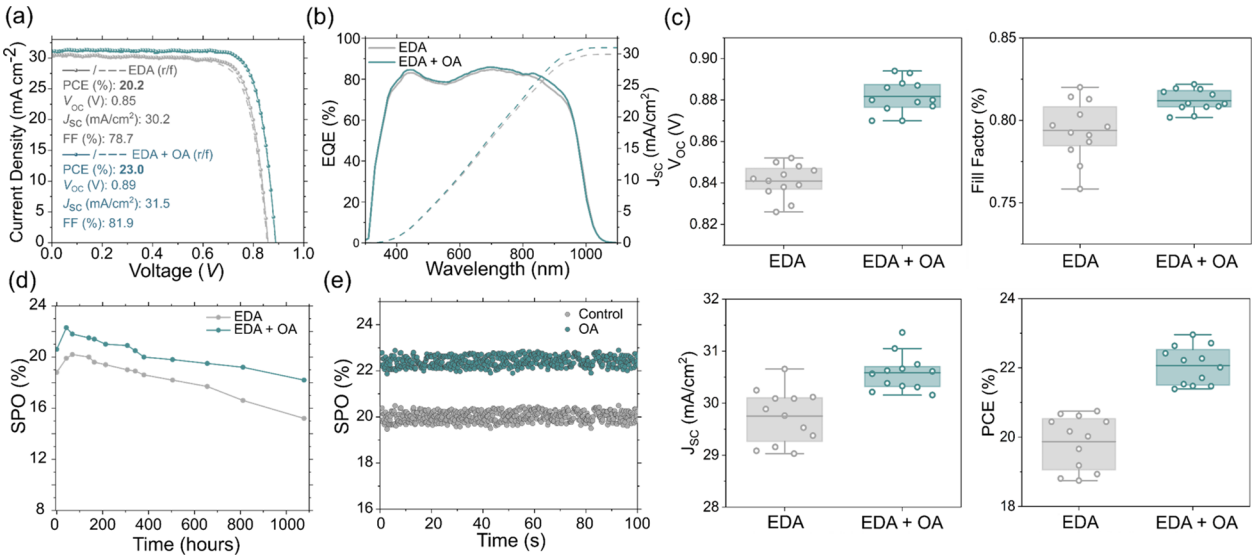

Figure 3. Characterization of NBG perovskite solar cells. (a) $J-V$ curves of control (EDA) and OA treated NBG devices (EDA+OA). (b) EQE measurements of EDA and EDA+OA treated devices. (c) Photovoltaic parameters of 12 EDA and EDA+OA treated devices. (d) Stabilized power output (SPO) of encapsulated EDA and EDA+OA treated devices stored in ambient air for 1100 h. (e) SPO of champion EDA and EDA+OA devices. Device active area was 0.049 cm^2.

as well as potential mitigation of Sn^{2+} oxidation. We found that the C 1s peak was significantly more intense after OA treatment, which we attribute to the long carbon chain of OA (Figure 2a). The total C:Sn peak area ratio also increased by 50% after OA treatment (Figure S8). The Sn $3d_{3/2}$ and $3d_{5/2}$ peaks exhibited a slight shift to a lower binding energy after OA treatment (Figure 2b), which we attribute to coordination of the carboxylic acid functional group with surface Sn^{2+} to form a metal carboxylate complex, a phenomenon that has been reported previously in high-efficiency Pb−Sn PSCs.[28,30] We also found that the Sn^{4+} content was reduced from 9.7% for EDA-treated films to 7.3% for EDA+OA-treated films.

We also carried out Fourier-transform infrared (FTIR) spectroscopy of untreated, EDA-treated, and EDA+OA-treated perovskite thin films to determine bonding interactions between the perovskite, EDA, and OA (Figure S9). We observe peaks that can be attributed to the presence of OA on the perovskite surface via excess CH_2 and C−O stretching signal, which is only observed for OA-treated films (Figure S9d,e). Furthermore, the C−O stretch peak appears to be shifted to a lower wavenumber for the OA-treated perovskite compared to the raw signal for OA. We attribute this shift to the carboxylic acid coordinate bonding with Sn^{2+}/Pb^{2+} on the surface of the perovskite,[28] which is in agreement with the shift to a lower binding energy of the Sn 3d core levels after OA surface treatment (Figure 2b).

To understand how post-treatment with OA affects the perovskite/C_{60} interface energetics we used ultraviolet photoelectron spectroscopy (UPS), finding that OA induces a 0.25 eV Fermi level upshift compared to control EDA-treated films, resulting in stronger surface n-type doping (Figure 2c,d, Figure S10). This change in the surface potential not only mitigates the detrimental surface oxidative p-doping associated with Sn-based perovskites, but also results in a reduction of the minority carrier concentration at the C_{60} interface.[17,25] This accords with the reduced nonradiative recombination evident in the PLQY and TRPL measurements of OA-treated films.

We then fabricated single-junction Pb−Sn PSCs to assess whether the reduction in nonradiative recombination at the perovskite/ETL interface translates to improved device performance, using a device structure of ITO/PEDOT:PSS/1.8 M $Cs_{0.05}FA_{0.7}MA_{0.25}Pb_{0.5}Sn_{0.5}I_3$ perovskite/C_{60}/BCP/Ag. Here we also compare control EDA-treated devices with OA-treated devices (EDA+OA). We first compared several orders of magnitude of concentrations for the OA post-treatment to find the optimal concentration (Figures S11 and S12). After optimizing the OA concentration, we employed the combined EDA+OA post-treatment, achieving a V_{OC} of 0.89 V and PCE of 23.0% (22.4% stabilized) (Figure 3a,e). We posit that the combination of EDA and OA passivation works better than either treatment individually due to their opposite charge and thus affinity toward different surface sites on the perovskite. While it has been suggested that an ammonium group from EDA^{2+} will interact broadly with acceptor-type defects,[25] prior reports along with our FTIR and XPS results suggest that OA selectively coordinates the B-site cations of the perovskite via the carboxylic acid functional group.[28,30] We therefore attribute the synergistic effects of the combined EDA+OA passivation to the complementary surface binding.

External quantum efficiency (EQE) measurements revealed a slight improvement in J_{SC} relative to control devices (30.7 mA/cm^2 vs 30.0 mA/cm^2), with most of the improvement arising from the wavelength region of ∼900−1000 nm (Figure 3b). We therefore conclude that the OA layer on the perovskite surface is thin enough that carrier extraction is not inhibited.

Photovoltaic parameters of NBG devices with and without OA treatment are shown in Figure 3c, demonstrating a consistent all-around performance improvement, especially with regard to device V_{OC}. EDA and EDA+OA treated devices exhibited a champion stabilized power output (SPO) of 20.0% and 22.4%, respectively (Figure 3e). Encapsulated EDA and EDA+OA treated devices retained 81% and 88% of their respective initial efficiency after 1100 h storage in ambient air (RT, ∼ 50% relative humidity, Figure 3d).

We then sought to incorporate our high-V_{OC} OA-treated NBG active layer in monolithic all-perovskite tandem solar cells in combination with a $Cs_{0.2}FA_{0.8}Pb(I_{0.6}Br_{0.4})_3$ of ∼1.8 eV

https://doi.org/10.1021/acsenergylett.3c02470
ACS Energy Lett. 2024, 9, 520−527

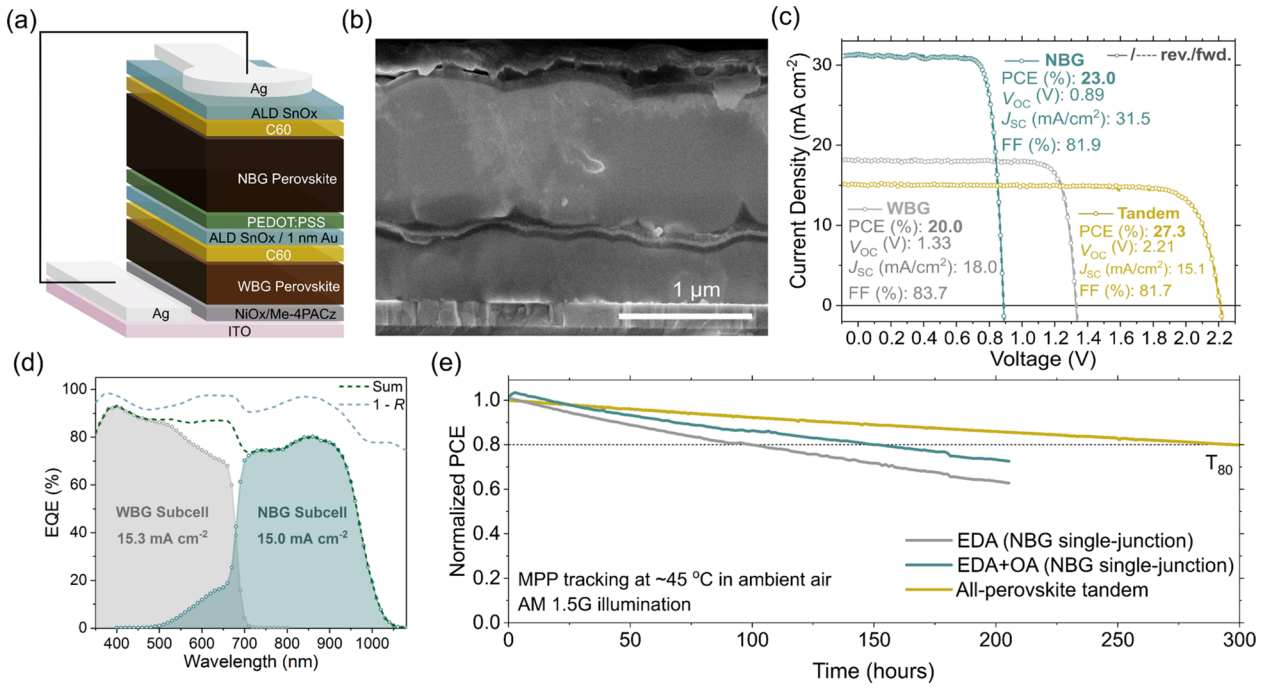

Figure 4. Monolithic all-perovskite tandem solar cells. (a) Schematic diagram of all-perovskite tandem device structure. (b) Cross-sectional SEM image of tandem device. (c) *J*–*V* curves of champion WBG, NBG, and tandem devices. Device active area was 0.049 cm^2. (d) EQE measurements of WBG and NBG subcells within the tandem device. (e) Maximum power point (MPP) tracking of single-junction NBG devices and all-perovskite tandems under continuous AM1.5G illumination. Devices were encapsulated, and MPP tracking was carried out under ambient conditions without cooling (~45 °C, ~50% RH). Initial tandem PCE was 26.2%.

WBG perovskite (see details in Methods). The tandem device structure was ITO/NiOx/Me-4PACz/WBG perovskite/C_{60}/ALD SnOx/Au (1 nm)/PEDOT:PSS/NBG perovskite/C_{60}/ALD SnOx/Ag (Figure 4a), with the SEM cross-sectional image showing the ~1 μm thick Pb–Sn perovskite layer necessary for optimal current matching (Figure 4b).[8] Figure 4c shows forward and reverse *J*–*V* scans of champion WBG, NBG, and tandem PSCs. We report a PCE of 27.3% with a high V_{OC} of 2.21 V, along with a J_{SC} of 15.1 mA/cm^2 and an FF of 81.7%. We sent a tandem cell to an accredited independent photovoltaic calibration laboratory (Japan Electrical Safety and Environment Technology Laboratories, JET). The device delivered a certified stabilized PCE of 26.4% and a V_{OC} of 2.17 V (Figure S13).

From EQE measurements of each subcell, we obtained integrated short-circuit current density (J_{SC}) values of 15.3 and 15.0 mA/cm^2 for the WBG and NBG subcells, respectively (Figure 4d). The bandgaps of the WBG and NBG subcells calculated from the EQE spectra were 1.79 and 1.24 eV, respectively. We note that the efficiency of the tandems remains limited by the J_{SC}, which is limited by that of the NBG subcell and significantly lower than the highest reported values of >16.5 mA/cm^2.[8] Optical losses for wavelengths greater than ~650 nm are primarily attributable to parasitic absorption by the interconnecting layer (SnOx/Au/PEDOT:PSS herein), as well as the J_{SC} deficit of ~1.2 eV PbSn perovskites. These losses are expected to be minimized by replacing SnOx/Au with a more optically transparent layer such as indium zinc oxide (IZO) and/or replacing PEDOT:PSS with a self-assembled monolayer HTL. Additionally, given that the oxidation of Sn-containing perovskite is particularly harmful to device J_{SC}, further advances in device encapsulation and surface oxidation suppression are expected to result in reduced optical losses.

The tandems retain 80% of their initial PCE after ~300 h of continuous operation under AM1.5G illumination without cooling, while the OA-treated single-junction NBG devices retain 80% of their initial PCE after ~150 h (Figure 4e). We attribute the improved stability of the tandems relative to the single-junction NBG subcell to the reduced exposure of the NBG subcell to near-UV light due to absorption by the top WBG subcell. Encapsulated tandem devices stored in the dark in ambient air for 300 h exhibited negligible losses in PCE (Figure S15).

In summary, we offer a strategy for the mitigation of harmful perovskite/ETL interfacial recombination by introducing long-chain OA ligands between adjacent layers. The OA surface treatment has the added benefits of Sn^{2+} coordination along with n-doping, resulting in significantly improved device V_{OC}, enabling high-efficiency all-perovskite tandems and demonstrating an important step toward the application of all-perovskite tandem solar cells.

■ ASSOCIATED CONTENT

Data Availability Statement

All data are available in the main text or Supporting Information.

Supporting Information

The Supporting Information is available free of charge at https://pubs.acs.org/doi/10.1021/acsenergylett.3c02470.

Experimental section, materials and methods, additional device statistics and certification, structural and optoelectronic characterization of perovskite surface and bulk (Supplementary Figures S1–S15, Supplementary Table S1, and Supplementary Note 1) (PDF)

https://doi.org/10.1021/acsenergylett.3c02470
ACS Energy Lett. 2024, 9, 520–527

AUTHOR INFORMATION

Corresponding Authors

Bin Chen − *The Edward S. Rogers Department of Electrical and Computer Engineering, University of Toronto, Toronto, Ontario M5S 3G4, Canada; Department of Chemistry, Northwestern University, Evanston, Illinois 60208, United States;* orcid.org/0000-0002-2106-7664; Email: bin.chen@northwestern.edu

Edward H. Sargent − *The Edward S. Rogers Department of Electrical and Computer Engineering, University of Toronto, Toronto, Ontario M5S 3G4, Canada; Department of Chemistry, Northwestern University, Evanston, Illinois 60208, United States; Department of Electrical and Computer Engineering, Northwestern University, Evanston, Illinois 60208, United States;* orcid.org/0000-0003-0396-6495; Email: ted.sargent@utoronto.ca

Authors

Aidan Maxwell − *The Edward S. Rogers Department of Electrical and Computer Engineering, University of Toronto, Toronto, Ontario M5S 3G4, Canada;* orcid.org/0000-0001-5826-6598

Hao Chen − *The Edward S. Rogers Department of Electrical and Computer Engineering, University of Toronto, Toronto, Ontario M5S 3G4, Canada*

Luke Grater − *The Edward S. Rogers Department of Electrical and Computer Engineering, University of Toronto, Toronto, Ontario M5S 3G4, Canada;* orcid.org/0000-0001-5920-4022

Chongwen Li − *The Edward S. Rogers Department of Electrical and Computer Engineering, University of Toronto, Toronto, Ontario M5S 3G4, Canada*

Sam Teale − *The Edward S. Rogers Department of Electrical and Computer Engineering, University of Toronto, Toronto, Ontario M5S 3G4, Canada;* orcid.org/0000-0001-9638-3453

Junke Wang − *The Edward S. Rogers Department of Electrical and Computer Engineering, University of Toronto, Toronto, Ontario M5S 3G4, Canada*

Lewei Zeng − *The Edward S. Rogers Department of Electrical and Computer Engineering, University of Toronto, Toronto, Ontario M5S 3G4, Canada*

Zaiwei Wang − *The Edward S. Rogers Department of Electrical and Computer Engineering, University of Toronto, Toronto, Ontario M5S 3G4, Canada*

So Min Park − *The Edward S. Rogers Department of Electrical and Computer Engineering, University of Toronto, Toronto, Ontario M5S 3G4, Canada*

Maral Vafaie − *The Edward S. Rogers Department of Electrical and Computer Engineering, University of Toronto, Toronto, Ontario M5S 3G4, Canada;* orcid.org/0000-0001-9119-6499

Siraj Sidhik − *Department of Material Science and Nanoengineering and Department of Chemical and Biomolecular Engineering, Rice University, Houston, Texas 77005, United States*

Isaac W. Metcalf − *Department of Material Science and Nanoengineering and Department of Chemical and Biomolecular Engineering, Rice University, Houston, Texas 77005, United States*

Yanjiang Liu − *The Edward S. Rogers Department of Electrical and Computer Engineering, University of Toronto, Toronto, Ontario M5S 3G4, Canada;* orcid.org/0000-0002-6119-2793

Aditya D. Mohite − *Department of Material Science and Nanoengineering and Department of Chemical and Biomolecular Engineering, Rice University, Houston, Texas 77005, United States;* orcid.org/0000-0001-8865-409X

Complete contact information is available at: https://pubs.acs.org/10.1021/acsenergylett.3c02470

Author Contributions

†A.M. and H.C. contributed equally.

Author Contributions

A.M. conceived the idea and wrote the original draft. A.M., H.C., C.L., S.T., and B.C. planned and coordinated the experimental work. A.M. fabricated the narrow bandgap devices and tandems and fabricated the perovskite films for characterizations. H.C. fabricated the wide bandgap devices, and the tandems for certification. L.G., C.L., and S.T. carried out optical spectroscopy of films and devices and data analysis. L.G. carried out UPS measurements and data analysis. Y.L. carried out XPS measurements and data analysis. S.S. and I.W.M. carried out GIWAXS measurements and analyzed the data. J.W., Z.W., L.Z., and S.M.P. helped optimize the single-junction and tandem device structure. M.V. carried out FTIR measurements. B.C., S.T., and C.L. assisted with device analysis and data interpretation. E.H.S. and A.D.M. secured funding and helped to review and edit the manuscript.

Funding

This research was made possible by the US Department of the Navy, Office of Naval Research Grant (N00014-20-1-2572). This work was supported in part by the Ontario Research Fund-Research Excellence program (ORF7 ministry of Research and Innovation, Ontario Research Fund-Research Excellence Round 7). This work was also supported by the Natural Sciences and Engineering Council of Canada.

Notes

The authors declare no competing financial interest.

ACKNOWLEDGMENTS

The authors thank Esther Tsai for assisting with GIWAXS measurements. This research used the beamline 11-BM of the National Synchrotron Light Source II, a U.S. Department of Energy (DOE) Office of Science user facility operated for the DOE Office of Science by Brookhaven National Laboratory under Contract No. DE-SC0012704.

REFERENCES

(1) Chen, W.; Zhu, Y.; Xiu, J.; Chen, G.; Liang, H.; Liu, S.; Xue, H.; Birgersson, E.; Ho, J. W.; Qin, X.; Lin, J.; Ma, R.; Liu, T.; He, Y.; Ng, A. M. C.; Guo, X.; He, Z.; Yan, H.; Djurišić, A. B.; Hou, Y. Monolithic Perovskite/Organic Tandem Solar Cells with 23.6% Efficiency Enabled by Reduced Voltage Losses and Optimized Interconnecting Layer. *Nature Energy 2022 7:3* **2022**, *7* (3), 229−237.

(2) Al-Ashouri, A.; Köhnen, E.; Li, B.; Magomedov, A.; Hempel, H.; Caprioglio, P.; Márquez, J. A.; Vilches, A. B. M.; Kasparavicius, E.; Smith, J. A.; Phung, N.; Menzel, D.; Grischek, M.; Kegelmann, L.; Skroblin, D.; Gollwitzer, C.; Malinauskas, T.; Jošt, M.; Matič, G.; Rech, B.; Schlatmann, R.; Topič, M.; Korte, L.; Abate, A.; Stannowski, B.; Neher, D.; Stolterfoht, M.; Unold, T.; Getautis, V.; Albrecht, S. Monolithic Perovskite/Silicon Tandem Solar Cell with > 29% Efficiency by Enhanced Hole Extraction. *Science (1979)* **2020**, *370* (6522), 1300−1309.

(3) Lin, R.; Xiao, K.; Qin, Z.; Han, Q.; Zhang, C.; Wei, M.; Saidaminov, M. I.; Gao, Y.; Xu, J.; Xiao, M.; Li, A.; Zhu, J.; Sargent, E. H.; Tan, H. Monolithic All-Perovskite Tandem Solar Cells with 24.8% Efficiency Exploiting Comproportionation to Suppress Sn(II) Oxidation in Precursor Ink. *Nature Energy 2019 4:10* **2019**, *4* (10), 864−873.
(4) Wang, R.; Huang, T.; Xue, J.; Tong, J.; Zhu, K.; Yang, Y. Prospects for Metal Halide Perovskite-Based Tandem Solar Cells. *Nature Photonics 2021 15:6* **2021**, *15* (6), 411−425.
(5) Yang, Z.; Yu, Z.; Wei, H.; Xiao, X.; Ni, Z.; Chen, B.; Deng, Y.; Habisreutinger, S. N.; Chen, X.; Wang, K.; Zhao, J.; Rudd, P. N.; Berry, J. J.; Beard, M. C.; Huang, J. Enhancing Electron Diffusion Length in Narrow-Bandgap Perovskites for Efficient Monolithic Perovskite Tandem Solar Cells. *Nature Communications 2019 10:1* **2019**, *10* (1), 1−9.
(6) Tong, J.; Song, Z.; Kim, D. H.; Chen, X.; Chen, C.; Palmstrom, A. F.; Ndione, P. F.; Reese, M. O.; Dunfield, S. P.; Reid, O. G.; Liu, J.; Zhang, F.; Harvey, S. P.; Li, Z.; Christensen, S. T.; Teeter, G.; Zhao, D.; Al-Jassim, M. M.; van Hest, M. F. A. M.; Beard, M. C.; Shaheen, S. E.; Berry, J. J.; Yan, Y.; Zhu, K. Carrier Lifetimes of > 1 Ms in Sn-Pb Perovskites Enable Efficient All-Perovskite Tandem Solar Cells. *Science (1979)* **2019**, *364* (6439), 475−479.
(7) Wen, J.; Zhao, Y.; Liu, Z.; Gao, H.; Lin, R.; Wan, S.; Ji, C.; Xiao, K.; Gao, Y.; Tian, Y.; Xie, J.; Brabec, C. J.; Tan, H. Steric Engineering Enables Efficient and Photostable Wide-Bandgap Perovskites for All-Perovskite Tandem Solar Cells. *Adv. Mater.* **2022**, *34*, 2110356.
(8) Lin, R.; Xu, J.; Wei, M.; Wang, Y.; Qin, Z.; Liu, Z.; Wu, J.; Xiao, K.; Chen, B.; Park, S. M.; Chen, G.; Atapattu, H. R.; Graham, K. R.; Xu, J.; Zhu, J.; Li, L.; Zhang, C.; Sargent, E. H.; Tan, H. All-Perovskite Tandem Solar Cells with Improved Grain Surface Passivation. *Nature 2022 603:7899* **2022**, *603* (7899), 73−78.
(9) *Best Research-Cell Efficiency Chart | Photovoltaic Research | NREL*. https://www.nrel.gov/pv/cell-efficiency.html (accessed 2022-05-09).
(10) Chen, H.; Maxwell, A.; Li, C.; Teale, S.; Chen, B.; Zhu, T.; Ugur, E.; Harrison, G.; Grater, L.; Wang, J.; Wang, Z.; Zeng, L.; Park, S. M.; Chen, L.; Serles, P.; Awni, R. A.; Subedi, B.; Zheng, X.; Xiao, C.; Podraza, N. J.; Filleter, T.; Liu, C.; Yang, Y.; Luther, J. M.; De Wolf, S.; Kanatzidis, M. G.; Yan, Y.; Sargent, E. H. Regulating Surface Potential Maximizes Voltage in All-Perovskite Tandems. *Nature 2022 613:7945* **2023**, *613* (7945), 676−681.
(11) Leijtens, T.; Bush, K. A.; Prasanna, R.; McGehee, M. D. Opportunities and Challenges for Tandem Solar Cells Using Metal Halide Perovskite Semiconductors. *Nature Energy 2018 3:10* **2018**, *3* (10), 828−838.
(12) Rajagopal, A.; Yang, Z.; Jo, S. B.; Braly, I. L.; Liang, P. W.; Hillhouse, H. W.; Jen, A. K. Y. Highly Efficient Perovskite-Perovskite Tandem Solar Cells Reaching 80% of the Theoretical Limit in Photovoltage. *Adv. Mater.* **2017**, *29* (34), 1702140.
(13) Jošt, M.; Kegelmann, L.; Korte, L.; Albrecht, S. Monolithic Perovskite Tandem Solar Cells: A Review of the Present Status and Advanced Characterization Methods Toward 30% Efficiency. *Adv. Energy Mater.* **2020**, *10* (26), 1904102 DOI: 10.1002/aenm.201904102.
(14) Warby, J.; Zu, F.; Zeiske, S.; Gutierrez-Partida, E.; Frohloff, L.; Kahmann, S.; Frohna, K.; Mosconi, E.; Radicchi, E.; Lang, F.; Shah, S.; Peña-Camargo, F.; Hempel, H.; Unold, T.; Koch, N.; Armin, A.; De Angelis, F.; Stranks, S. D.; Neher, D.; Stolterfoht, M. Understanding Performance Limiting Interfacial Recombination in Pin Perovskite Solar Cells. *Adv. Energy Mater.* **2022**, *12* (12), 2103567.
(15) Oliver, R. D. J.; Caprioglio, P.; Peña-Camargo, F.; Buizza, L. R. V.; Zu, F.; Ramadan, A. J.; Motti, S. G.; Mahesh, S.; McCarthy, M. M.; Warby, J. H.; Lin, Y.-H.; Koch, N.; Albrecht, S.; Herz, L. M.; Johnston, M. B.; Neher, D.; Stolterfoht, M.; Snaith, H. J. Understanding and Suppressing Non-Radiative Losses in Methylammonium-Free Wide-Bandgap Perovskite Solar Cells. *Energy Environ. Sci.* **2022**, *15* (2), 714−726.
(16) Menzel, D.; Al-Ashouri, A.; Tejada, A.; Levine, I.; Guerra, J. A.; Rech, B.; Albrecht, S.; Korte, L. Field Effect Passivation in Perovskite Solar Cells by a LiF Interlayer. *Adv. Energy Mater.* **2022**, *12* (30), 2201109.
(17) Kapil, G.; Bessho, T.; Maekawa, T.; Baranwal, A. K.; Zhang, Y.; Kamarudin, M. A.; Hirotani, D.; Shen, Q.; Segawa, H.; Hayase, S. Tin-Lead Perovskite Fabricated via Ethylenediamine Interlayer Guides to the Solar Cell Efficiency of 21.74%. *Adv. Energy Mater.* **2021**, *11* (25), 2101069.
(18) Liu, J.; De Bastiani, M.; Aydin, E.; Harrison, G. T.; Gao, Y.; Pradhan, R. R.; Eswaran, M. K.; Mandal, M.; Yan, W.; Seitkhan, A.; Babics, M.; Subbiah, A. S.; Ugur, E.; Xu, F.; Xu, L.; Wang, M.; ur Rehman, A.; Razzaq, A.; Kang, J.; Azmi, R.; Said, A. A.; Isikgor, F. H.; Allen, T. G.; Andrienko, D.; Schwingenschlögl, U.; Laquai, F.; De Wolf, S. Efficient and Stable Perovskite-Silicon Tandem Solar Cells through Contact Displacement by MgFx. *Science (1979)* **2022**, *377* (6603), 302−306.
(19) Zhang, K.; Forberich, K.; Lüer, L.; Cerrillo, G.; Meng, W.; Du, X.; le Corre, V. M.; Zhao, Y.; Niu, T.; Xue, Q.; Koster, L. J. A.; Li, N.; Brabec, C. J. Understanding the Limitations of Charge Transporting Layers in Mixed Lead-Tin Halide Perovskite Solar Cells. *Advanced Energy and Sustainability Research* **2022**, *3* (3), 2100156.
(20) Lanzetta, L.; Webb, T.; Zibouche, N.; Liang, X.; Ding, D.; Min, G.; Westbrook, R. J. E.; Gaggio, B.; Macdonald, T. J.; Islam, M. S.; Haque, S. A. Degradation Mechanism of Hybrid Tin-Based Perovskite Solar Cells and the Critical Role of Tin (IV) Iodide. *Nature Communications 2021 12:1* **2021**, *12* (1), 1−11.
(21) Pitaro, M.; Tekelenburg, E. K.; Shao, S.; Loi, M. A. Tin Halide Perovskites: From Fundamental Properties to Solar Cells. *Adv. Mater.* **2022**, *34* (1), 2105844.
(22) Lanzetta, L.; Aristidou, N.; Haque, S. A. Stability of Lead and Tin Halide Perovskites: The Link between Defects and Degradation. *J. Phys. Chem. Lett.* **2020**, *11* (2), 574−585.
(23) Liang, Z.; Xu, H.; Zhang, Y.; Liu, G.; Chu, S.; Tao, Y.; Xu, X.; Xu, S.; Zhang, L.; Chen, X.; Xu, B.; Xiao, Z.; Pan, X.; Ye, J. A Selective Targeting Anchor Strategy Affords Efficient and Stable Ideal-Bandgap Perovskite Solar Cells. *Adv. Mater.* **2022**, *34* (18), 2110241.
(24) Yan, N.; Ren, X.; Fang, Z.; Jiang, X.; Xu, Z.; Zhang, L.; Ren, S.; Jia, L.; Zhang, J.; Du, Y.; Zhao, D.; Zhao, K.; Yang, S.; Liu, S. Ligand-Anchoring-Induced Oriented Crystal Growth for High-Efficiency Lead-Tin Perovskite Solar Cells. *Adv. Funct Mater.* **2022**, *32* (27), 2201384.
(25) Hu, S.; Otsuka, K.; Murdey, R.; Nakamura, T.; Truong, M. A.; Yamada, T.; Handa, T.; Matsuda, K.; Nakano, K.; Sato, A.; Marumoto, K.; Tajima, K.; Kanemitsu, Y.; Wakamiya, A. Optimized Carrier Extraction at Interfaces for 23.6% Efficient Tin-Lead Perovskite Solar Cells. *Energy Environ. Sci.* **2022**, *15* (5), 2096−2107.
(26) Lu, J.; Jiang, L.; Li, W.; Li, F.; Pai, N. K.; Scully, A. D.; Tsai, C. M.; Bach, U.; Simonov, A. N.; Cheng, Y. B.; Spiccia, L. Diammonium and Monoammonium Mixed-Organic-Cation Perovskites for High Performance Solar Cells with Improved Stability. *Adv. Energy Mater.* **2017**, *7* (18), 1700444.
(27) Jeong, M.; Choi, I. W.; Go, E. M.; Cho, Y.; Kim, M.; Lee, B.; Jeong, S.; Jo, Y.; Choi, H. W.; Lee, J.; Bae, J. H.; Kwak, S. K.; Kim, D. S.; Yang, C. Stable Perovskite Solar Cells with Efficiency Exceeding 24.8% and 0.3-V Voltage Loss. *Science (1979)* **2020**, *369* (6511), 1615.
(28) Liu, H.; Wang, L.; Li, R.; Shi, B.; Wang, P.; Zhao, Y.; Zhang, X. Modulated Crystallization and Reduced VOCDeficit of Mixed Lead-Tin Perovskite Solar Cells with Antioxidant Caffeic Acid. *ACS Energy Lett.* **2021**, *6* (8), 2907−2916.
(29) Guan, L.; Jiao, N.; Guo, Y. Trap-State Passivation by Nonvolatile Small Molecules with Carboxylic Acid Groups for Efficient Planar Perovskite Solar Cells. *J. Phys. Chem. C* **2019**, *123* (23), 14223−14228.
(30) Hu, S.; Truong, M. A.; Otsuka, K.; Handa, T.; Yamada, T.; Nishikubo, R.; Iwasaki, Y.; Saeki, A.; Murdey, R.; Kanemitsu, Y.; Wakamiya, A. Mixed Lead-Tin Perovskite Films with > 7 Ms Charge Carrier Lifetimes Realized by Maltol Post-Treatment. *Chem. Sci.* **2021**, *12* (40), 13513−13519.

(31) Hu, L.; Wang, C.; Kennedy, R. M.; Marks, L. D.; Poeppelmeier, K. R. The Role of Oleic Acid: From Synthesis to Assembly of Perovskite Nanocuboid Two-Dimensional Arrays. *Inorg. Chem.* **2015**, *54* (3), 740−745.
(32) Andreakou, P.; Brossard, M.; Li, C.; Bernechea, M.; Konstantatos, G.; Lagoudakis, P. G. Size- and Temperature-Dependent Carrier Dynamics in Oleic Acid Capped PbS Quantum Dots. *J. Phys. Chem. C* **2013**, *117* (4), 1887−1892.
(33) Li, Z.; Zhu, Y. Surface-Modification of SiO2 Nanoparticles with Oleic Acid. *Appl. Surf. Sci.* **2003**, *211* (1−4), 315−320.
(34) Zhang, L.; He, R.; Gu, H. C. Oleic Acid Coating on the Monodisperse Magnetite Nanoparticles. *Appl. Surf. Sci.* **2006**, *253* (5), 2611−2617.
(35) Abdelmageed, G.; Sully, H. R.; Bonabi Naghadeh, S.; El-Hag Ali, A.; Carter, S. A.; Zhang, J. Z. Improved Stability of Organometal Halide Perovskite Films and Solar Cells toward Humidity via Surface Passivation with Oleic Acid. *ACS Appl. Energy Mater.* **2018**, *1* (2), 387−392.
(36) Zhang, M.; Li, W.; Zhao, W.; Han, X. Enhancing Charge Carrier Transport in the Carbon-Electrode-Based CsPbI2Br Perovskite Solar Cells via I/Br Homogenization Process Modulation and Oleic Acid Surface Passivation. *ACS Appl. Energy Mater.* **2023**, *6* (5), 2973−2980.
(37) Kirchartz, T.; Márquez, J. A.; Stolterfoht, M.; Unold, T. Photoluminescence-Based Characterization of Halide Perovskites for Photovoltaics. *Adv. Energy Mater.* **2020**, *10* (26), 1904134.
(38) Chen, H.; Teale, S.; Chen, B.; Hou, Y.; Grater, L.; Zhu, T.; Bertens, K.; Park, S. M.; Atapattu, H. R.; Gao, Y.; Wei, M.; Johnston, A. K.; Zhou, Q.; Xu, K.; Yu, D.; Han, C.; Cui, T.; Jung, E. H.; Zhou, C.; Zhou, W.; Proppe, A. H.; Hoogland, S.; Laquai, F.; Filleter, T.; Graham, K. R.; Ning, Z.; Sargent, E. H. Quantum-size-tuned heterostructures enable efficient and stable inverted perovskite solar cells. *Nat. Photonics* **2022**, *16*, 352−358.

https://doi.org/10.1021/acsenergylett.3c02470
ACS Energy Lett. 2024, 9, 520−527